Meson exchange currents in neutron-proton bremsstrahlung

Yi Li
College of Physics and Technology, Guangxi University, Nanning, Guangxi 530004, People's Republic of China

M. K. Liou
Department of Physics and Institute for Nuclear Theory, Brooklyn College of the City University of New York, Brooklyn, New York 11210, USA

W. M. Schreiber
Department of Physics, College of Staten Island of the City University of New York, Staten Island, New York 10314, USA

B. F. Gibson
Theoretical Division, Los Alamos National Laboratory, Los Alamos, New Mexico 87545, USA

R. G. E. Timmermans
Theory Group, Kernfysisch Versneller Instituut, University of Groningen Zernikelaan 25, NL-9747 AA Groningen, The Netherlands
(Received 26 June 2007; published 4 April 2008)

Background: The meson exchange current (MEC) contribution is important in the neutron-proton bremsstrahlung process ($np\gamma$) when the two nucleon-scattering angles are small. However, our understanding of such effects is limited, and the reason why meson exchange current effects dominate the $np\gamma$ cross section has not been thoroughly investigated. **Purpose**: The primary focus of this investigation is to understand the origin of the MEC contribution, to identify the leading MEC amplitudes, and to comprehend why these MEC amplitudes dominate the $np\gamma$ cross sections. **Method**: We used a new method that combines the one-boson-exchange (OBE) approach with the soft-photon approach to define 10 different $np\gamma$ amplitudes. These amplitudes are used to calculate $np\gamma$ cross sections at 225 MeV for nucleon laboratory scattering angles lying between 12° and 43°. The results of these calculations are then compared to investigate the meson exchange current effect in $np\gamma$. **Results**: (i) The OBE amplitude $M^{\rm PS}_{np\gamma,\mu}$ and the two-u-two-t special (TuTts) soft-photon amplitude $M^{\rm TuTts}_{np\gamma,\mu}$ predict quantitatively similar $np\gamma$ cross sections. (ii) The MEC effect is found to be significant when the two nucleon-scattering angles are far from the elastic limit (45°), but the effect is insignificant when the nucleon angles approach the elastic limit. (iii) The origin of the MEC effect and the leading MEC amplitudes have been identified in this investigation. Furthermore, the reason is now clear why the leading MEC amplitudes dominate the $np\gamma$ cross section when the nucleon-scattering angles are small. (iv) The contribution from the anomalous magnetic moments of the proton and the neutron is confirmed to be negligibly small. (v) In general, the theoretical cross sections using the amplitude $M^{\rm PS}_{np\gamma,\mu}$, or the amplitude $M^{\rm TuTts}_{np\gamma,\mu}$, are consistent with the triple differential cross sections recently measured at the Los Alamos National Laboratory. However, there exists an unexplained discrepancy between theory and experiment in some cases. **Conclusions**: The findings of this investigation have enhanced our understanding of the meson exchange current effect in $np\gamma$. The comparative amplitude method introduced can be used for other bremsstrahlung investigations.

DOI: 10.1103/PhysRevC.77.044001 PACS number(s): 21.30.−x, 24.80.+y, 25.40.Cm, 25.40.Dn

I. INTRODUCTION

Recently, the first triple differential cross section for the neutron-proton bremsstrahlung ($np\gamma$) process was published [1]. The $np\gamma$ process, unlike the proton-proton bremsstrahlung ($pp\gamma$) process, is sensitive to the exchange of charged mesons mediating the nucleon-nucleon interaction. In this work we explore the origin of the dominance of the meson exchange current (MEC) diagrams in the $np\gamma$ cross section.

The MEC effect in the $np\gamma$ process has been investigated by many authors using various models and approximations. Most previous investigations focused on the nonrelativistic potential-model approach [2–5]. To motivate our use of a relativistic approach in this work and to identify the differences between our approach and the potential-model approach, we briefly review what was learned from Refs. [2–5]. We use that opportunity to compare the findings of Ref. [2] and Refs. [3–5] and to provide an alternative physical interpretation of the conclusion regarding MEC effects obtained in Ref. [3].

In the potential model the $np\gamma$ amplitude can be defined from an electromagnetic potential $V_{\rm em}$ that is composed of two terms: $V^1_{\rm em}$ and $V^2_{\rm em}$. (We follow the notation of Ref. [2]). The potential $V^1_{\rm em}$ is generated from the coupling of the electromagnetic field to the nucleon currents, whereas the potential $V^2_{\rm em}$ is generated from the coupling of the electromagnetic field to the MEC. Starting from potential $V^1_{\rm em}$, one can define an external amplitude $\vec{M}_E(V^1_{\rm em})$ and a rescattering amplitude $\vec{M}_R(V^1_{\rm em})$. It was shown in Ref. [2] that $\vec{M}_R(V^1_{\rm em})$ can be separated into two amplitudes, $\vec{M}_{R0}(V^1_{\rm em})$ and $\vec{M}_{R1}(V^1_{\rm em})$, plus higher-order $O(K)$ terms, to derive the low-energy theorem. {Note: $\vec{M}_R(V^1_{\rm em}) =$

$\vec{M}_{R0}(V^1_{\rm em}) + \vec{M}_{R1}(V^1_{\rm em}) + O(K)$ [2].} Similarly, the potential $V^2_{\rm em}$ can be used to define the MEC amplitude $\vec{M}_X(V^2_{\rm em})$. The internal amplitude $\vec{M}_I$ is equal to the sum of $\vec{M}_R(V^1_{\rm em})$ and $\vec{M}_X(V^2_{\rm em})$. The total amplitude $\vec{M}_T$, which combines $\vec{M}_E(V^1_{\rm em})$ and $\vec{M}_I$, can be written as the sum of the four amplitudes $\vec{M}_E(V^1_{\rm em})$, $\vec{M}_{R0}(V^1_{\rm em})$, $\vec{M}_{R1}(V^1_{\rm em})$, and $\vec{M}_X(V^2_{\rm em})$, if higher-order terms $O(K)$ are omitted. This total amplitude $\vec{M}_T$ was used in Ref. [2] to prove that it satisfies the soft-photon theorem (the low-energy theorem). Furthermore, the same $\vec{M}_T$ (but including some other higher-order terms in the photon energy K) has also been used by the authors of Refs. [3,4] to calculate $np\gamma$ cross sections and to study the MEC effect in $np\gamma$. Some important results and implications can be summarized as follows:

(i) It is well known that the soft-photon theorem is a fundamental theorem for all bremsstrahlung processes. Any valid bremsstrahlung amplitude must satisfy this theorem. In Ref. [2] [using the potential $V^2_{\rm em}$ defined in Eq. (7)], it is proven that the total amplitude $\vec{M}_T$ used in the potential-model approach is, indeed, consistent with (obeys) the soft-photon theorem. This results because the rescattering amplitude $\vec{M}_{R1}(V^1_{\rm em})$ precisely cancels the MEC amplitude $\vec{M}_X(V^2_{\rm em})$ [i.e., the "cancellation condition" is $\vec{M}_{R1}(V^1_{\rm em}) + \vec{M}_X(V^2_{\rm em}) \equiv 0$]. Therefore, the final form of the total amplitude $\vec{M}_T$ actually includes only the external amplitude $\vec{M}_E(V^1_{\rm em})$ and the internal amplitude $\vec{M}_{R0}(V^1_{\rm em})$. It should be emphasized that this expression for $\vec{M}_T$ is independent of the potential $V^2_{\rm em}$ that generates $\vec{M}_X(V^2_{\rm em})$. This result from Ref. [2] has the following implications: (A) In the potential-model approach the $np\gamma$ total amplitude $\vec{M}_T$ can be expressed in two different ways. The *first expression* for $\vec{M}_T$ is the sum of $\vec{M}_E(V^1_{\rm em})$, $\vec{M}_R(V^1_{\rm em})$, and $\vec{M}_X(V^2_{\rm em})$. The *second expression* for $\vec{M}_T$ is the sum of $\vec{M}_E(V^1_{\rm em})$ and $\vec{M}_{R0}(V^1_{\rm em})$. The equality of the two expressions occurs because $\vec{M}_{R0}(V^1_{\rm em})$ is equal to the sum of $\vec{M}_R(V^1_{\rm em})$ and $\vec{M}_X(V^2_{\rm em})$. That is, we have $\vec{M}_{R0}(V^1_{\rm em}) = \vec{M}_R(V^1_{\rm em}) + \vec{M}_X(V^2_{\rm em})$. The *second expression* for $\vec{M}_T$, which is actually the soft-photon amplitude, depends on $\vec{M}_X(V^2_{\rm em})$ only implicitly (indirectly). Another important point is that the small contribution from the rescattering amplitude $\vec{M}_R(V^1_{\rm em})$ does not imply that the individual contributions from $\vec{M}_{R0}(V^1_{\rm em})$ and $\vec{M}_{R1}(V^1_{\rm em})$ must be small. Both can have similar large amplitudes but differ in sign. This is indeed the case for the $np\gamma$ process. (B) The *second expression* for $\vec{M}_T$ $[=\vec{M}_E(V^1_{\rm em}) + \vec{M}_{R0}(V^1_{\rm em})]$ demonstrates that a soft-photon amplitude can be constructed by using Low's prescription (or a modified Low prescription). The internal amplitude in this soft-photon approach can be obtained entirely from the external amplitude by imposing the "gauge invariant condition." In other words, because of the "cancellation condition," the amplitude $\vec{M}_X(V^2_{\rm em})$ does not play a direct role in the derivation of the soft-photon amplitude. The relativistic soft-photon amplitude used in this work for the study of the MEC effect in $np\gamma$ is a good example. However, there is a disadvantage in using the soft-photon amplitude to investigate MEC effects in $np\gamma$. It is difficult to identify the precise MEC contribution from a soft-photon amplitude, because the amplitude does not involve an explicit MEC amplitude. (C) Any $np\gamma$ amplitude (in the potential-model approach) that does not satisfy the "cancellation condition" violates the soft-photon theorem. For example, as pointed out in Ref. [2], an amplitude that includes only the exact $\vec{M}_E(V^1_{\rm em})$ and $\vec{M}_R(V^1_{\rm em})$ would not be a valid amplitude, because it would violate current conservation.

(ii) The *first expression* for the total amplitude $\vec{M}_T$ (but including some higher-order terms in K) was used by Brown and Franklin [3] to calculate $np\gamma$ cross sections and to investigate the MEC effect in $np\gamma$. Specific conclusions from their calculations relevant to this discussion were:

(a) The contribution from the rescattering amplitude $\vec{M}_R(V^1_{\rm em})$ was small, about 10%.

(b) The contribution from the MEC amplitude $\vec{M}_X(V^2_{\rm em})$ was significant; more precisely, the cross section calculated using the external amplitude $\vec{M}_E(V^1_{\rm em})$ plus the MEC amplitude $\vec{M}_X(V^2_{\rm em})$ was more than two times larger than that calculated using $\vec{M}_E(V^1_{\rm em})$ alone.

(c) The contribution from the sum of the two amplitudes $\vec{M}_E(V^1_{\rm em})$ and $\vec{M}_X(V^2_{\rm em})$ dominated the exact cross section calculated from the total amplitude $\vec{M}_T$.

Most of those findings were confirmed by Herrmann, Speth, and Nakayama [4] and by Nakayama [5], although the latter calculations omitted the rescattering amplitude $\vec{M}_R(V^1_{\rm em})$. If one compares these calculations with that which was demonstrated in Ref. [2], one may perceive that an apparent contradiction exists between Ref. [2] and Refs. [3–5]. For example, in Ref. [2] it was shown that the *second expression* for $\vec{M}_T$, which is consistent with the soft-photon theorem, is independent of $V^2_{\rm em}$. However, the *first expression* for $\vec{M}_T$, which involves the explicit MEC amplitude $\vec{M}_X(V^2_{\rm em})$ generated from $V^2_{\rm em}$, was used in Refs. [3–5]. Actually, there is no contradiction between Ref. [2] and Refs. [3,4]. The "cancellation condition," which was proved in Ref. [2], is an exact result, and it leads to the internal amplitude being defined to be $\vec{M}_{R0}(V^1_{\rm em})$, the sum of $\vec{M}_R(V^1_{\rm em})$ and $\vec{M}_X(V^2_{\rm em})$. The required cancellation of the two amplitudes $\vec{M}_{R1}(V^1_{\rm em})$ and $\vec{M}_X(V^2_{\rm em})$ occurs numerically in the calculations of Refs. [3,4]. The cancellation between $\vec{M}_X(V^2_{\rm em})$ and $\vec{M}_{R1}(V^1_{\rm em})$ is required to preserve current conservation. Because of this cancellation, the amplitude $\vec{M}_T$ used in Refs. [3,4] satisfies the fundamental soft-photon theorem. Furthermore, because $\vec{M}_R(V^1_{\rm em})$ is small, the internal amplitude $\vec{M}_{R0}(V^1_{\rm em})$ is approximately equal to the MEC amplitude $\vec{M}_X(V^2_{\rm em})$. That is, $\vec{M}_{R0}(V^1_{\rm em}) \approx \vec{M}_X(V^2_{\rm em})$ explains the conclusion regarding MEC effects in Ref. [3].

In addition to the potential-model approach, other approaches can be utilized to study the MEC effects in the $np\gamma$ process. Because each approach has advantages and limitations, more than one approach should be used to investigate the important MEC effect issue. Two additional approaches that utilize relativistic and gauge invariant bremsstrahlung amplitudes, the two-u-two-t special (TuTts) amplitude [6–10] and the one-boson-exchange (OBE) amplitude [11–14], were previously employed to investigate the photon emission mechanism governing the three $NN\gamma$ processes ($pp\gamma$, $np\gamma$, and $nn\gamma$) as well as noncoplanaroty effects in $pp\gamma$ and $np\gamma$. Using the TuTts amplitude, it was shown that MEC effects dominate the $np\gamma$ cross section when the scattering angles are small (i.e., when one is far from the elastic limit) [6,7]. A similar result can also be obtained from the OBE amplitude. These results confirm the finding of the potential-model approach. Nonetheless, the physical reason why MEC effects should dominate the $np\gamma$ cross section has not been thoroughly understood.

In this work we use a new method that combines the OBE approach and the soft-photon approach to define 10 different $np\gamma$ amplitudes (including the OBE amplitude $M^{\rm PS}_{np\gamma,\mu}$ [14], the TuTts amplitude $M^{\rm TuTts}_{\mu}$, and the other amplitudes derived from $M^{\rm PS}_{np\gamma,\mu}$). These amplitudes provide more direct information and precise definitions regarding MEC effects in $np\gamma$. We utilize them to calculate $np\gamma$ cross sections for the projectile energy of 225 MeV and for nucleon laboratory scattering angles lying between 12° and 43°. The primary focus of this investigation is to understand the origin of the large MEC effect, to identify the leading MEC terms, and to understand why these MEC terms dominate the $np\gamma$ cross section.

II. $np\gamma$ AMPLITUDES

The detailed expression for the $np\gamma$ amplitude $M^{\rm PS}_{np\gamma,\mu}$ [with the pion-nucleon coupling treated as a pseudoscalar (PS) interaction] can be found in Ref. [14]. This amplitude is obtained from two distinct sets of photon emission diagrams: the neutral-meson-exchange (NME) diagrams and the charged-meson-exchange (CME) diagrams. These two sets of diagrams are shown in Figs. 1(a), 1(b), and 1(c). In Fig. 1(a) we depict NME diagrams, which involve four different external photon emission processes. In these diagrams A^0 represents 10 different neutral mesons (π^0, ρ^0, δ^0, t_1^0, a_1^0, η, σ, ω, t_0, a_0) that can be exchanged between the proton p and the neutron n, $g_{p\mathrm{A}^0p}$ represents the coupling constant mediating the coupling of the meson A^0 to the pp current, $g_{n\mathrm{A}^0n}$ represents the coupling constant mediating the coupling of the meson A^0 to the nn current, and $\lambda^\alpha(\alpha = 1, 2, 3, 4, 5)$ represents the five Fermi covariants. Other factors, which are irrelevant to our investigation, are suppressed. All NME diagrams can contribute to generate an amplitude $M^{\rm NME}_{\mu}$. This amplitude may depend on many fundamental constants. In this investigation, however, we focus on the following: the proton charge e, the square of the coupling constants $g^2_{\mathrm{A}^0}$, and the anomalous magnetic moments of the proton κ_p and the neutron κ_n. Following isospin symmetry (charge independence), we define

$$g_{\mathrm{A}^0} = |g_{p\mathrm{A}^0p}| = |g_{n\mathrm{A}^0n}|. \tag{1}$$

Thus, the amplitude $M^{\rm NME}_{\mu}$ can be expressed as a function of $g^2_{\mathrm{A}^0}$, e, κ_p, and κ_n:

$$M^{\rm NME}_{\mu} \equiv \sum_{A^0} M^{\rm NME}_{\mu}\left(g^2_{\mathrm{A}^0}, e, \kappa_p, \kappa_n\right). \tag{2}$$

It satisfies the gauge condition $M^{\rm NME}_{\mu} K^{\mu} = 0$.

There are two types of CME diagrams. We refer to the first kind as the external CME diagrams, because they involve only external photon emission, and to the second kind as the internal CME diagrams, because they involve only internal photon emission. The external CME diagrams are depicted in Fig. 1(b). In the processes represented by these diagrams, an incoming proton converts into an outgoing neutron by emitting a charged meson A^+ or an incoming neutron converts into an outgoing proton by absorbing a charged meson A^+. Here the A^+ represents any of the five possible charged mesons (π^+, ρ^+, δ^+, t_1^+, a_1^+) used in our OBE model. The $g_{p\mathrm{A}^+n}$ represents the coupling constant connecting the charged meson A^+ to the $(p-n)$ vertex, whereas the $g_{n\mathrm{A}^+p}$ represents the coupling constant connecting the charged meson A^+ to the $(n-p)$ vertex. The entire set of CME diagrams contributes to the generation of the external CME amplitude $M^{\rm CME}_{(E)\mu}$, which is a function of $g^2_{\mathrm{A}^+}$, e, κ_p, and κ_n. Here we assume that

$$g_{\mathrm{A}^+} = |g_{p\mathrm{A}^+n}| = |g_{n\mathrm{A}^+p}|. \tag{3}$$

Thus, we have

$$M^{\rm CME}_{(E)\mu} \equiv \sum_{A^+} M^{\rm CME}_{(E)\mu}\left(g^2_{\mathrm{A}^+}, e, \kappa_p, \kappa_n\right). \tag{4}$$

From isospin symmetry follows the important relationship between g_{A^+} and g_{A^0},

$$g_{\mathrm{A}^+} = \sqrt{2} g_{\mathrm{A}^0}, \tag{5}$$

for the five isotriplet mesons (π, ρ, δ, t_1, a_1). For example, if A^+ represents π^+ (or a_1^+), then A^0 represents π^0 (or a_1^0). Thus, for these mesons we can write

$$M^{\rm CME}_{(E)\mu}\left(g^2_{\mathrm{A}^+}, e, \kappa_p, \kappa_n\right) = M^{\rm CME}_{(E)\mu}\left(2g^2_{\mathrm{A}^0}, e, \kappa_p, \kappa_n\right). \tag{6}$$

Finally, we illustrate the internal CME diagrams in Fig. 1(c). The symbols used in Fig. 1(c) are identical to those used in Fig. 1(b). The important difference between these two figures is that the photon is emitted from the external nucleon line in Fig. 1(b), whereas the photon is emitted from the exchanged (internal) charged meson A^+ in Fig. 1(c). The diagrams in Fig. 1(c) illustrate the MEC effects contributing to $np\gamma$. Note that the diagrams in Fig. 1(c) also include the contribution from the extra gauge factors that are required for current conservation. See Eq. (14) of Ref. [14]. Again, these internal CME diagrams can be used to generate an internal CME amplitude $M^{\rm CME}_{(I)\mu}$, which is a function of $g^2_{\mathrm{A}^+}$ and e,

$$M^{\rm CME}_{(I)\mu} \equiv \sum_{A^+} M^{\rm CME}_{(I)\mu}\left(g^2_{\mathrm{A}^+}, e\right). \tag{7}$$

For the five mesons (π, ρ, δ, t_1, a_1) we may also write

$$M^{\rm CME}_{(I)\mu}\left(g^2_{\mathrm{A}^+}, e\right) = M^{\rm CME}_{(I)\mu}\left(2g^2_{\mathrm{A}^0}, e\right). \tag{8}$$

The complete CME amplitude can then be expressed as

$$M^{\rm CME}_{\mu} \equiv M^{\rm CME}_{(E)\mu} + M^{\rm CME}_{(I)\mu} \tag{9}$$

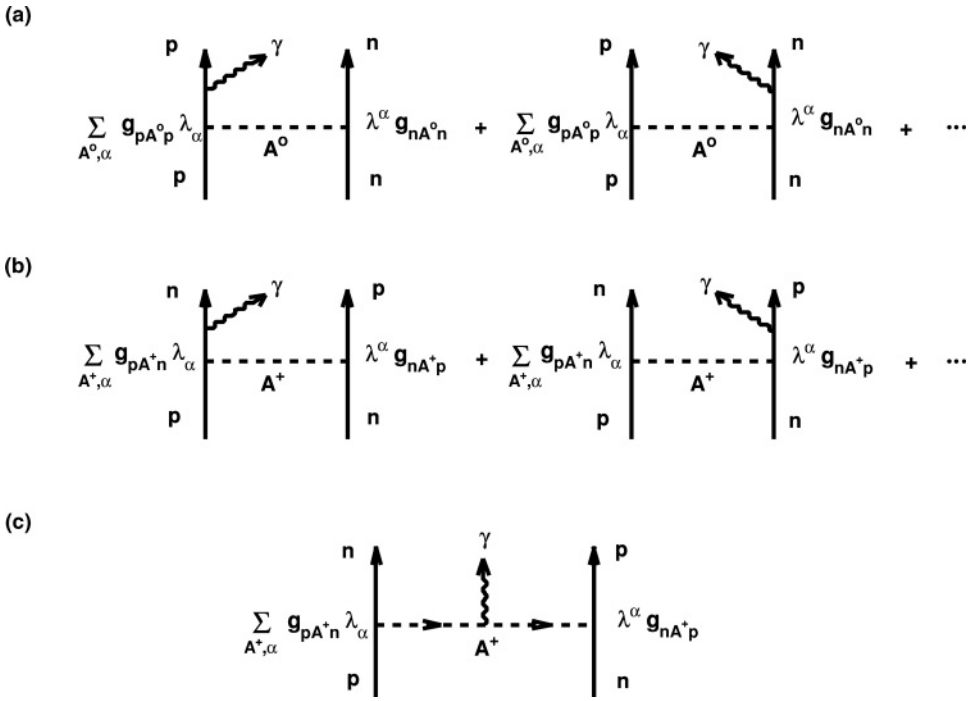

FIG. 1. Diagrams for the $np\gamma$ process: (a) neutral-meson exchange (NME) diagrams; (b) external emission charged-meson exchange (CME) diagrams; (c) internal emission charged-meson exchange (CME) diagrams.

$$= \sum_{A^+} \left[M^{\rm CME}_{(E)\mu}\left(g^2_{A^+} = 2g^2_{\rm A^0}, e, \kappa_p, \kappa_n\right) + M^{\rm CME}_{(I)\mu}\left(g^2_{A^+} = 2g^2_{\rm A^0}, e\right)\right]. \quad (10)$$

The amplitude $M^{\rm CME}_\mu$ satisfies the gauge condition,

$$M^{\rm CME}_\mu K^\mu = 0. \quad (11)$$

The total $np\gamma$ amplitude $M^{\rm PS}_{np\gamma,\mu}$ can be obtained by combining Eq. (2) for $M^{\rm NME}_\mu$ and Eq. (9) [or Eq. (10)] for $M^{\rm CME}_\mu$,

$$M^{\rm PS}_{np\gamma,\mu} \equiv M^{\rm NME}_\mu + M^{\rm CME}_\mu \quad (12)$$

$$= \sum_{A^0} M^{\rm NME}_\mu\left(g^2_{\rm A^0}, e, \kappa_p, \kappa_n\right) + \sum_{A^+} \left[M^{\rm CME}_{(E)\mu}\left(g^2_{A^+} = 2g^2_{\rm A^0}, e, \kappa_p, \kappa_n\right) + M^{\rm CME}_{(I)\mu}\left(g^2_{A^+} = 2g^2_{\rm A^0}, e\right)\right]. \quad (13)$$

Here, $M^{\rm NME}_\mu$ involves all 10 neutral mesons and $M^{\rm CME}_\mu$ involves only the 5 charged mesons (π^+, ρ^+, δ^+, t_1^+, a_1^+). To investigate the MEC effect in the absence of the anomalous magnetic moment effect, we define the following additional $np\gamma$ amplitudes:

(i) We define an amplitude $M^{(1)}_\mu$ that is identical to the expression for $M^{\rm PS}_{np\gamma,\mu}$ given by Eq. (13) except that it has $\kappa_p = \kappa_n = 0$; that is,

$$M^{(1)}_\mu = \left(M^{\rm PS}_{np\gamma,\mu}\right)_{\kappa_p=\kappa_n=0}. \quad (14)$$

(ii) Replacing $g_{\rm A^+}$ given by Eq. (5), we define a new amplitude $M^{(2)}_\mu$ that can be expressed in terms of the substitution

$$g_{\rm A^+} \to g_{\rm A^0}. \quad (15)$$

That is, $M^{(2)}_\mu$ is defined by

$$M^{(2)}_\mu = \left(M^{\rm PS}_{np\gamma,\mu}\right)_{g^2_{\rm A^+}\to g^2_{\rm A^0}} = \sum_{A^0} M^{\rm NME}_\mu\left(g^2_{\rm A^0}, e, \kappa_p, \kappa_n\right) + \sum_{A^+} \left[M^{\rm CME}_{(E)\mu}\left(g^2_{A^+} \to g^2_{\rm A^0}, e, \kappa_p, \kappa_n\right) + M^{\rm CME}_{(I)\mu}\left(g^2_{A^+} \to g^2_{\rm A^0}, e\right)\right]. \quad (16)$$

(iii) We define an amplitude $M^{(3)}_\mu$ that can be expressed in terms of $M^{\rm CME}_\mu$ given by Eq. (10) but with $\kappa_p = \kappa_n = 0$,

$$M^{(3)}_\mu = \left(M^{\rm CME}_\mu\right)_{\kappa_p=\kappa_n=0}. \quad (17)$$

(iv) The leading external amplitude, which we define to be $M^{(4)}_\mu$, was used in Refs. [6,7] in investigating the MEC effect. The derivation of this amplitude in our OBE model differs somewhat from that given in Refs. [6,7]. Six Mandelstam variables (two "s," two "t," and two "u") can be defined for the $np\gamma$ process. The variables $\bar{s}$, $\bar{t}$, and $\bar{u}$ are the averages of the two "s," two "t," and two "u" variables, respectively. They satisfy the on-shell condition

$$\bar{s} + \bar{t} + \bar{u} = 4m^2, \quad (18)$$

where m is the nucleon mass, which we define to be the average of the proton mass and the neutron mass in our calculations. If we choose ($\bar{s}$, $\bar{t}$, $\bar{u}$) to be the on-shell

point and expand the amplitude $M^{\rm PS}_{np\gamma,\mu}$ about this point, then we can obtain the following soft-photon expansion:

$$M^{\rm PS}_{np\gamma,\mu} = \frac{A_\mu(\bar{u},\bar{t})}{K} + B_\mu(\bar{u},\bar{t}) + C_\mu(\bar{u},\bar{t})K + \cdots. \tag{19}$$

Here, $A_\mu(\bar{u},\bar{t})$ involves only the leading external contribution (photon emission from the proton charge e) from the amplitudes $M^{\rm NME}_\mu$ and $M^{\rm CME}_{(E)\mu}$, whereas $B_\mu(\bar{u},\bar{t})$ and $C_\mu(\bar{u},\bar{t})$ include contributions from all three amplitudes, $M^{\rm NME}_\mu$, $M^{\rm CME}_{(E)\mu}$, and $M^{\rm CME}_{(I)\mu}$. In other words, the bremsstrahlung contribution from the meson exchange currents and the anomalous magnetic moments is found in the second term $[B_\mu(\bar{u},\bar{t})]$ plus the higher-order terms of the soft-photon expansion given by Eq. (19). We define the leading ampliitude $M^{(4)}_\mu$ to be the leading term of the soft-photon expansion,

$$M^{(4)}_\mu = A_\mu(\bar{u},\bar{t})/K, \tag{20}$$

which satisfies the gauge condition $M^{(4)}_\mu K^\mu = 0$. The first two terms of the soft-photon expansion can be used to define a soft-photon amplitude

$$M^{\rm SPA}_\mu = M^{(4)}_\mu + B_\mu(\bar{u},\bar{t}). \tag{21}$$

Following the method used in Refs. [6,7], one can ascertain that the amplitude $M^{\rm SPA}_\mu$ can be used to investigate MEC effects. However, it is not transparent to use that method to explain why the MEC contributiuon dominates the $np\gamma$ cross section. That is the primary reason we used the OBE amplitude approach in this investigation.

Note that our model does not include photon emission processes involving an internal pion emitting a photon and converting to either a ρ or ω meson. We anticipate that the contributions from such processes will be small in the kinematic region considered in this work.

III. RESULTS AND DISCUSSION

To investigate the meson exchange current effect in the $np\gamma$ process, we use eight amplitudes $\{M^{\rm PS}_{np\gamma,\mu}$ given in Eq. (13) or Eq. (10) of Ref. [14], $M^{\rm NME}_\mu$ given in Eq. (2), $M^{\rm CME}_\mu$ given in Eq. (10), $M^{(1)}_\mu$ given in Eq. (14), $M^{(2)}_\mu$ given in Eq. (16), $M^{(3)}_\mu$ given in Eq. (17), $M^{(4)}_\mu$ given in Eq. (20), and $M^{\rm TuTts}_\mu$ given in Eq. (13) of Ref. [7]$\}$ to calculate coplanar $np\gamma$ cross sections $d^3\sigma/d\Omega_n d\Omega_p d\psi_\gamma$ as functions of the photon angle ψ_γ for a laboratory incident neutron energy of 225 MeV and for laboratory scattering angles lying between 12° and 43°. We use Horowitz's OBE parameters at 200 MeV [12,15] for the calculation of all $np\gamma$ cross sections. Some of these calculations are shown in Figs. 2–5.

(i) In Fig. 2 we compare calculated $np\gamma$ cross sections with experimental data [1]. The amplitudes used in the calculation of these theoretical cross sections are $M^{\rm PS}_{np\gamma,\mu}$ (the solid curve), $M^{(1)}_\mu$ (the dotted curve), $M^{\rm TuTts}_\mu$ (the dashed curve), and $M^{(4)}_\mu$ (the dashed-dotted curve). The physical values, $\kappa_p = 1.793$ and $\kappa_n = -1.913$, are used in the amplitudes $M^{\rm PS}_{np\gamma,\mu}$ and $M^{\rm TuTts}_\mu$, whereas the amplitudes $M^{(1)}_\mu$ and $M^{(4)}_\mu$ are independent of κ_p and κ_n. Recall that $M^{(1)}_\mu$ is defined in terms of $M^{\rm PS}_{np\gamma,\mu}$ by setting $\kappa_p = \kappa_n = 0$ and $M^{(4)}_\mu$ is the leading amplitude. Several interesting features of this figure and the physical implications of the results can be summarized as follows:

(a) A comparison of the solid curves with the dashed curves demonstrates clearly that the two amplitudes $M^{\rm PS}_{np\gamma,\mu}$ and $M^{\rm TuTts}_\mu$ predict quantitatively similar $np\gamma$ cross sections. In our recent investigation of the $pp\gamma$ process [13], we also found good agreement between the OBE amplitude (in particular, the pseudoscalar amplitude) and the TuTts amplitude when these two amplitudes were used to describe the KVI cross-section data [13]. Thus, we find, in general, that these two relativistic approaches (the OBE approach and the TuTts soft-photon approach) exhibit similar predictive power.

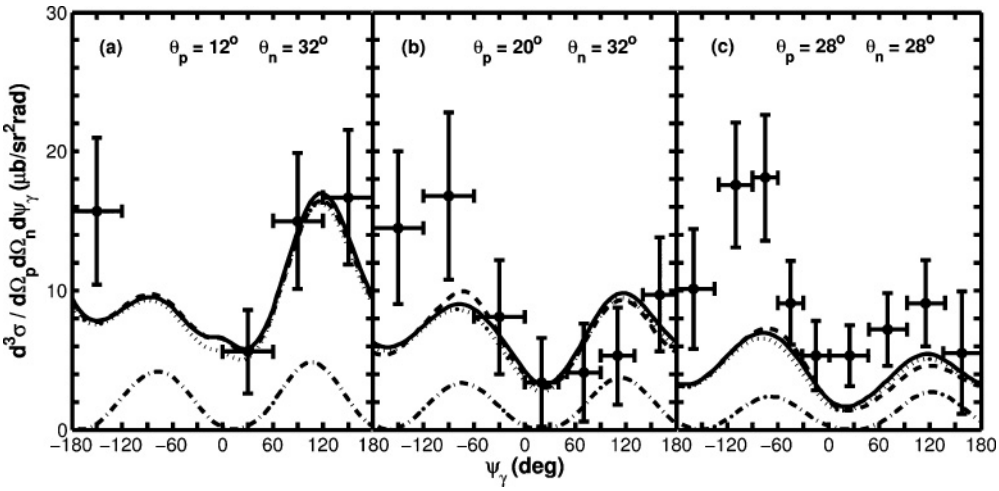

FIG. 2. Calculated $np\gamma$ cross sections and experimental data from Ref. [1]. The solid, dotted, dashed, and dashed-dotted curves were obtained using the amplitudes $M^{\rm PS}_{np\gamma,\mu}$, $M^{(1)}_\mu$, $M^{\rm TuTts}_\mu$, and $M^{(4)}_\mu$, respectively.

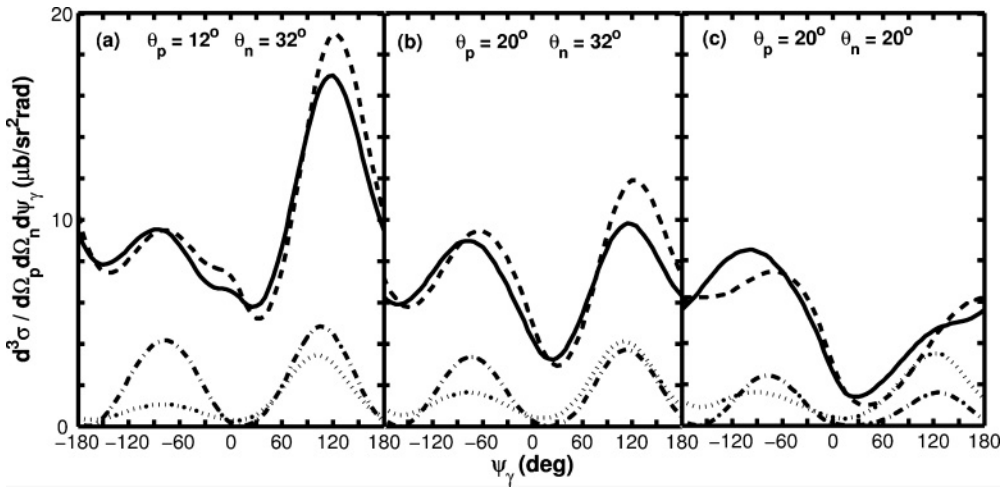

FIG. 3. Calculated $np\gamma$ cross sections for the scattering angles denoted, as a function of ψ_γ. The solid, dotted, dashed, and dashed-dotted curves were obtained using the amplitudes $M^{\rm PS}_{np\gamma,\mu}$, $M^{\rm NME}_{\mu}$, $M^{\rm CME}_{\mu}$, and $M^{(4)}_{\mu}$, respectively.

(b) If we compare the solid curves with the dotted curves, then we can ascertain that the anomalous magnetic moment contribution from κ_n and κ_p is negligibly small, confirming an important finding in Refs. [6,7] that the anomalous magnetic moments play an insignificant role in the $np\gamma$ process. Therefore, we have shown that

$$M^{(1)}_{\mu} \simeq M^{\rm PS}_{np\gamma,\mu} \simeq M^{\rm TuTs}_{\mu}. \tag{22}$$

(c) By comparing the dashed-dotted curves with the solid curves, it is obvious that the contribution from the amplitude $M^{(4)}_{\mu}$ [the leading term in the soft-photon expansion given by Eq. (19)] is small when each nucleon scattering angle (θ_n, θ_p) is less than 32°. This fact supports the findings of Refs. [6,7] that the contribution from the second term of the soft-photon expansion [B_μ of Eq. (19)], which involves the MEC effect, dominates the $np\gamma$ cross section for those cases involving small nucleon-scattering angles. This also implies that the cross section difference between the calculations using the $M^{\rm PS}_{np\gamma,\mu}$ amplitude (solid curves) and that using the $M^{(4)}_{\mu}$ amplitude (dashed-dotted curves) can be used to estimate the size of the MEC effect. In general, our investigation shows that (1) the cross section difference is large when each nucleon-scattering angle is small and that (2) the difference decreases as the nucleon-scattering angles increase. As will be shown in Fig. 4(b), such a difference approaches zero when each scattering angle tends toward 45°, the elastic limit. Thus, near the elastic limit ($\theta_n = \theta_p > 40°$) the contribution from the MEC becomes insignificant and the amplitude $M^{(4)}_{\mu}$ dominates the $np\gamma$ cross section, just as is predicted by the soft-photon theorem. However, one cannot use the cross-section difference between the solid curve and the dashed-dotted curve alone to understand why

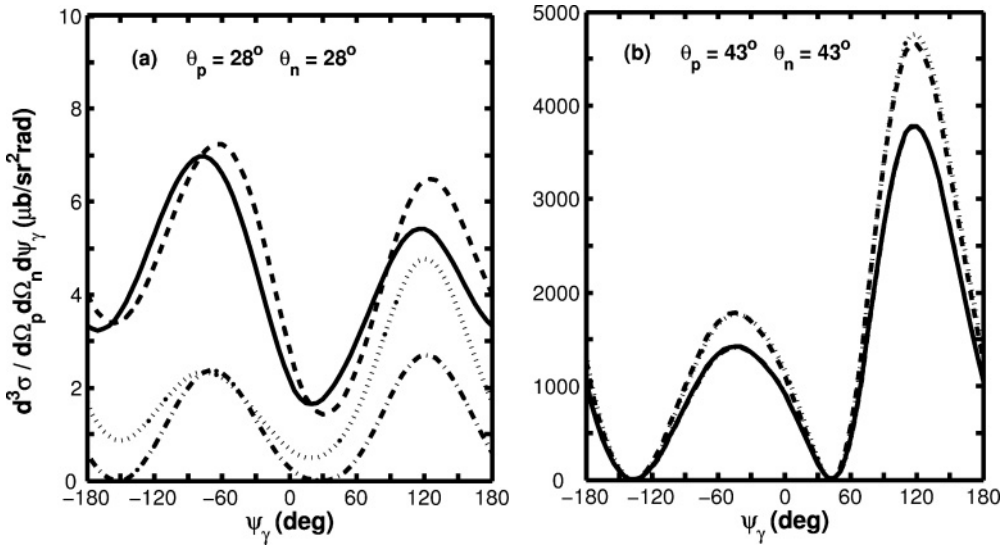

FIG. 4. Same as described in the caption to Fig. 3 but for different sets of scattering angles.

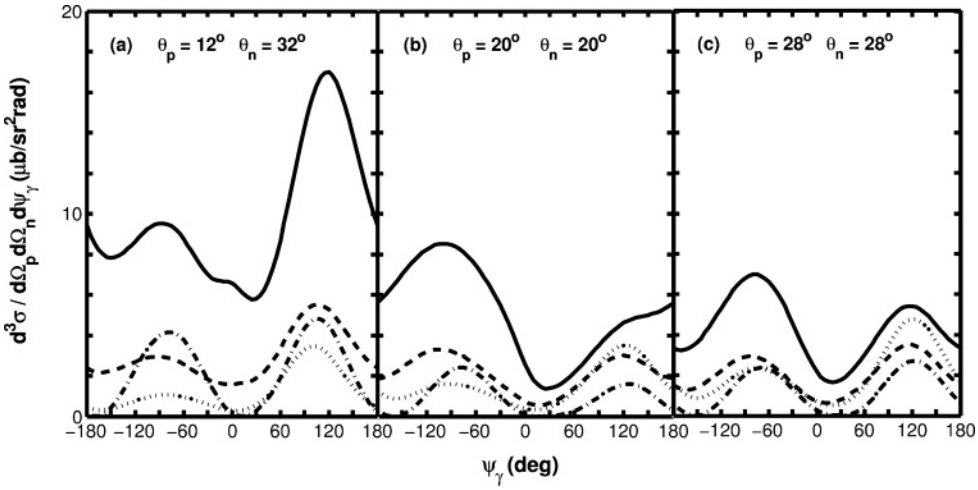

FIG. 5. Calculated $np\gamma$ cross sections for the scattering angles denoted as a function of ψ_γ. The solid, dashed, dotted, and dashed-dotted curves were obtained using the amplitudes $M^{\rm PS}_{np\gamma,\mu}$, $M^{(2)}_\mu$, $M^{\rm NME}_\mu$, and $M^{(4)}_\mu$, respectively.

the MEC contribution dominates the $np\gamma$ cross-section for small-angle scattering cases.

(d) In general, even though our theoretical calculations (solid, dashed, and dotted curves) are consistent with the experimental data [1], there exists a large discrepancy between theory and experiment for some cases with photon angles ψ_γ in the range $-180^\circ < \psi_\gamma < -60^\circ$. (In this range, the emitted photons that have relatively lower energies are found on the neutron side.) The cause remains unclear. However, to the best of our knowledge, all theoretical calculations (relativistic or nonrelativistic [3–5]) that are consistent with the fundamental soft-photon theorem predict similar $np\gamma$ cross sections. That is, there are no large discrepancies among the theoretical calculations. It seems unlikely that all of these theoretical models would suffer the same fundamental deficiency.

(ii) In Figs. 3 and 4, we present coplanar $np\gamma$ cross sections calculated using amplitudes $M^{\rm PS}_{np\gamma,\mu}$ (solid curves), $M^{\rm NME}_\mu$ (dotted curves), $M^{\rm CME}_\mu$ (dashed curves), and $M^{(4)}_\mu$ (dashed-dotted curves) as a function of ψ_γ at 225 MeV for $(\theta_p, \theta_n) = (12^\circ, 32^\circ)$, $(20^\circ, 32^\circ)$, $(20^\circ, 20^\circ)$, $(28^\circ, 28^\circ)$, and $(43^\circ, 43^\circ)$. These two figures provide the first elucidation of the separate contributions to the $np\gamma$ cross sections of the four major amplitudes. Let us summarize their interesting features and important physical implications:

(a) To provide a transparent analysis, let us introduce two useful soft-photon expansions:

$$M^{\rm NME}_\mu = \frac{A^{\rm NME}_\mu}{K} + B^{\rm NME}_\mu + C^{\rm NME}_\mu K + \cdots \tag{23}$$

and

$$M^{\rm CME}_\mu = \frac{A^{\rm CME}_\mu}{K} + B^{\rm CME}_\mu + C^{\rm CME}_\mu K + \cdots . \tag{24}$$

From these two expansions, one can see that

$$M^{\rm PS}_{np\gamma,\mu} = M^{\rm NME}_\mu + M^{\rm CME}_\mu \tag{25}$$

$$= \frac{A_\mu}{K} + B_\mu + C_\mu K + \cdots , \tag{26}$$

where

$$A_\mu = A^{\rm NME}_\mu + A^{\rm CME}_\mu , \tag{27}$$

$$B_\mu = B^{\rm NME}_\mu + B^{\rm CME}_\mu , \tag{28}$$

$$C_\mu = C^{\rm NME}_\mu + C^{\rm CME}_\mu , \tag{29}$$

and

$$M^{(4)}_\mu = \frac{A_\mu}{K} \tag{30}$$

$$= \frac{1}{K}\left(A^{\rm NME}_\mu + A^{\rm CME}_\mu\right). \tag{31}$$

Here A_μ, B_μ, C_μ, $A^{\rm NME}_\mu$, $B^{\rm NME}_\mu$, $C^{\rm NME}_\mu$, $A^{\rm CME}_\mu$, $B^{\rm CME}_\mu$, and $C^{\rm CME}_\mu$ are all functions of $\bar{u}$ and $\bar{t}$. The content of Eq. (25) is the same as that of Eq. (12), Eq. (26) is the same as Eq. (19), and Eq. (30) is the same as Eq. (20).

(b) In Fig. 3 we compare the results of $np\gamma$ cross sections calculated using four different amplitudes for the three cases of $(\theta_p, \theta_n) = (12^\circ, 32^\circ)$, $(20^\circ, 32^\circ)$, and $(20^\circ, 20^\circ)$. In each case our comparison shows that the dashed curve (calculated using the $M^{\rm CME}_\mu$ amplitude) dominates the $np\gamma$ cross section and is consistently in much better agreement with the solid curve (calculated using the exact $M^{\rm PS}_{np\gamma,\mu}$ amplitude) than the other two curves calculated using the $M^{\rm NME}_\mu$ and $M^{(4)}_\mu$ amplitudes. These results have the following implications:

(1) Based on the analysis given in (a), the contributions from $A^{\rm CME}_\mu/K$, $A^{\rm NME}_\mu/K$, $B^{\rm NME}_\mu$, $C^{\rm NME}_\mu$ (and higher-order terms) should be small. Thus, the dominant contribution must come from the $B^{\rm CME}_\mu$ term. (It is unlikely to arise from $C^{\rm CME}_\mu$ and higher-order terms.) Note that the $B^{\rm CME}_\mu$ term depends on the anomalous magnetic moments κ_p and κ_n from the external emission contribution. However, the contribution from these moments is negligibly small in the $np\gamma$ process.

(2) It is well known that the amplitude $M^{\rm NME}_\mu$ contributes nothing to the MEC effect, because it is generated from the exchange of neutral mesons and involves only external emission. Similarly, the amplitude

$A_\mu^{\rm CME}/K$, which belongs to the external emission class, has nothing to do with the MEC effect. Thus, although the amplitude $M_\mu^{\rm CME}$, which is generated from the exchange of charged mesons, has been regarded as the meson exchange current amplitude, its leading meson exchange current contribution actually comes from the $B_\mu^{\rm CME}$ term of Eq. (24).

(3) The MEC effect is significant in each of the three cases shown in this figure.

(c) We can also see that there is some cancellation between contributions from the two amplitudes $M_\mu^{\rm NME}$ and $M_\mu^{\rm CME}$, because the dashed curve is slightly higher than the solid curve at some ψ_γ angles.

(d) We have exploited two different ways of investigating the MEC contribution in $np\gamma$, the first discussed in (i)(c) and the second discussed in (ii)(a) and (ii)(b). In both approaches the MEC effect is included in the second term (and higher-order terms) of the soft-photon expansions [i.e., the B_μ term of Eq. (19) or the $B_\mu^{\rm CME}$ term of Eq. (24)]. An important condition for any $np\gamma$ cross section to exhibit significant MEC effects is that the contribution from the leading amplitudes, both $A_\mu^{\rm CME}/K$ and $A_\mu^{\rm NME}/K$ [$M_\mu^{(4)} = (A_\mu^{\rm CME} + A_\mu^{\rm NME})/K$], must be small (insignificant). This condition is satisfied for those $np\gamma$ conditions with small nucleon scattering angles (i.e., when one is far from the elastic limit). In contrast, for those cases with nucleon scattering approaching the elastic limit, the MEC effect should become insignificant, simply because the contribution from both amplitudes $A_\mu^{\rm CME}/K$ and $A_\mu^{\rm NME}/K$ (and, therefore, $M_\mu^{(4)}$) completely dominate the $np\gamma$ cross section. Figure 4(b) is a good example illustrating this point.

(e) Figure 4(b) represents an $np\gamma$ cross section near the elastic-scattering limit, $(\theta_p, \theta_n) = (43^\circ, 43^\circ)$. We point out two interesting features:

(1) The dashed-dotted curve [$M_\mu^{(4)}$] appears to be identical to the solid curve ($M_{np\gamma,\mu}^{\rm PS}$). This is because the contribution from the leading amplitude $M_\mu^{(4)}$ completely dominates the $np\gamma$ cross section calculated using the exact amplitude $M_{np\gamma,\mu}^{\rm PS}$. In other words, $M_\mu^{(4)}$ is approximately equal to $M_{np\gamma,\mu}^{\rm PS}$.

(2) The dotted curve ($M_\mu^{\rm NME}$) is quantitatively similar to the dashed curve ($M_\mu^{\rm CME}$). There are three reasons for such excellent agreement between the two curves. First, the leading amplitude $A_\mu^{\rm CME}/K$ completely dominates the $np\gamma$ cross section calculated using the amplitude $M_\mu^{\rm CME}$. That is, $A_\mu^{\rm CME}/K$ is approximately equal to $M_\mu^{\rm CME}$. Second, the leading amplitude $A_\mu^{\rm NME}/K$ dominates the $np\gamma$ cross section calculated using the amplitude $M_\mu^{\rm NME}$. In other words, $A_\mu^{\rm NME}/K$ is approximately equal to $M_\mu^{\rm NME}$. Third, $|M_\mu^{\rm CME}\epsilon^\mu|^2$ is approximately equal to $|M_\mu^{\rm NME}\epsilon^\mu|^2$. Here ϵ^μ is the photon polarization four-vector. Thus, not only is the cross-section difference between the solid curve and the dashed-dotted curve zero, but also the cross section difference between the dashed curve and the dotted curve is nearly zero over the entire range of ψ_γ. This implies that the MEC contribution is completely negligible for the $np\gamma$ case with $\theta_p = \theta_n = 43^\circ$. Therefore, we conclude that MEC effects should play no role in the $np\gamma$ process near the elastic-scattering limit with $\theta_p, \theta_n \geqslant 43^\circ$.

(iii) In Fig. 5 we exhibit coplanar $np\gamma$ cross sections calculated using amplitudes $M_{np\gamma,\mu}^{\rm PS}$ (solid curves), $M_\mu^{(2)}$ (dashed curves), $M_\mu^{\rm NME}$ (dotted curves), and $M_\mu^{(4)}$ (dashed-dotted curves) as a function of ψ_γ at 225 MeV for $(\theta_p, \theta_n) = (12^\circ, 32^\circ)$, $(20^\circ, 20^\circ)$, and $(28^\circ, 28^\circ)$. Although the results are not shown in Fig. 5, we have also found that calculations using the amplitudes $M_\mu^{(3)}$ and $M_\mu^{(4)}$ yield quantitatively similar $np\gamma$ cross sections over the whole range of ψ_γ. This fact implies that the anomalous magnetic moment effect must play an insignificant role in the amplitude $M_\mu^{\rm CME}$, and hence the amplitude $B_\mu^{\rm CME}$ (and other higher-order amplitudes) should depend mainly on the MEC effect. As we have already mentioned, the primary focus of this investigation is to understand the origin of the MEC effect, to identify the leading MEC terms, and to understand why these MEC terms dominate the $np\gamma$ cross section when the two nucleon-scattering angles (θ_p and θ_n) are small. Using the knowledge gained from analyzing Figs. 2, 3, and 4, we conclude that the origin of the MEC effect and the dominant MEC terms have been identified. The amplitude $B_\mu^{\rm CME}$, the second term in the soft-photon expansion of the amplitude $M_\mu^{\rm CME}$, is the leading MEC term. An examination of Fig. 5 provides a transparent explanation of why the amplitude $M_\mu^{\rm CME}$ dominates the $np\gamma$ cross section when the two nucleon-scattering angles are small.

(a) The major difference between the two amplitudes $M_\mu^{\rm NME}$ and $M_\mu^{\rm CME}$ is that the former involves only the exchange of neutral mesons, whereas the latter involves entirely the exchange of positively charged mesons. In other words, $M_\mu^{\rm NME}$ depends on the square of the coupling constants $g_{{\rm A}^0}^2$, whereas $M_\mu^{\rm CME}$ depends on the square of the coupling constants $g_{{\rm A}^+}^2$. From Eq. (5) we find that $g_{{\rm A}^+}^2 = 2g_{{\rm A}^0}^2$. It is this important relationship that explains why the $np\gamma$ cross-section contribution arising from $M_\mu^{\rm CME}$ is much greater than the cross section contribution arising from $M_\mu^{\rm NME}$ for small nucleon-scattering angles.

(b) Because our model that involves up to 10 mesons is complex, consider first a simple example to illustrate our point: Consider a model composed only of π-meson exchange. In this case $M_\mu^{\rm NME}$ will be proportional to $g_{\pi^0}^2$, whereas $M_\mu^{\rm CME}$ will be proportional to $g_{\pi^+}^2$. The $np\gamma$ cross section, $\sigma(\pi^0)$, calculated using $M_\mu^{\rm NME}(g_{\pi^0}^2)$ will be proportional to $g_{\pi^0}^4$, whereas the cross section, $\sigma(\pi^+)$, calculated using $M_\mu^{\rm CME}(g_{\pi^+}^2)$ will be proportional to $g_{\pi^+}^4$. Because $g_{\pi^+} = \sqrt{2}g_{\pi^0}$, we have $g_{\pi^+}^4/g_{\pi^0}^4 = 4$. This implies that $\sigma(\pi^+) \sim 4\sigma(\pi^0)$. It is important that the reader understand that the ratio $R = \sigma(\pi^+)/[4\sigma(\pi^0)]$ is a function of

$\theta_p, \theta_n, \psi_\gamma, \kappa_p, \kappa_n$, and e; it is not a constant. For example, in the case of $(\theta_p, \theta_n) = (43^\circ, 43^\circ)$ R is approximately 1 over the range $-180^\circ \leqslant \psi_\gamma \leqslant 180^\circ$, but for $(12^\circ, 12^\circ)$, we find $0.42 \leqslant R \leqslant 8.09$ over the range in ψ_γ. This conclusion should be qualitatively correct for the complete calculation of the $np\gamma$ cross sections using the 10 neutral and 5 charged mesons. This is because, as noted above, the $np\gamma$ cross sections are dominated by the amplitude $M_\mu^{\rm CME}$ for scattering angles that are far from the elastic limit. In support of this argument, results of additional calculations are shown in Fig. 5 and discussed next.

(c) In Fig. 5 the solid curves are calculated using the amplitude $M_{npγ,\mu}^{\rm PS}$, which depends on $g_{\rm A^+}^2 = 2g_{\rm A^0}^2$. That is, $M_{npγ,\mu}^{\rm PS} = M_{npγ,\mu}^{\rm PS}(g_{\rm A^+}^2 = 2g_{\rm A^0}^2)$. However, the dashed curves are calculated using the amplitude $M_\mu^{(2)}$, which is identical to $M_{npγ,\mu}^{\rm PS}$ except that $g_{\rm A^+}^2$ has been replaced by $g_{\rm A^0}^2$. That is, $M_\mu^{(2)} = M_{npγ,\mu}^{\rm PS}(g_{\rm A^+}^2 \to g_{\rm A^0}^2)$. Figure 5 shows that the dashed curve, which is similar in size to the dotted curve and the dashed-dotted curve, is much smaller than the solid curve. This clearly shows that the $np\gamma$ cross section calculated using the amplitude $M_{npγ,\mu}^{\rm PS}$ would be greatly reduced if $g_{\rm A^+}^2$ were changed from $2g_{\rm A^0}^2$ to $g_{\rm A^0}^2$. We point out that this change affects only the amplitude $M_\mu^{\rm CME}$. Thus, the leading meson exchange current amplitude $B_\mu^{\rm CME}$ dominates the $np\gamma$ cross section for small-angle scattering primarily because of the fact that $g_{\rm A^+}^2 = 2g_{\rm A^0}^2$.

IV. CONCLUSION

In conclusion, the MEC effect in $np\gamma$ was investigated using a new method that combines the OBE approach with the soft-photon approach. The method comprises three elements: (i) as illustrated in Eq. (12), the exact OBE amplitude $M_{npγ,\mu}^{\rm PS}$ is separated into the two amplitudes $M_\mu^{\rm NME}$ and $M_\mu^{\rm CME}$. (ii) As defined in Eqs. (23), (24), and (26), three soft-photon expansions are introduced for $M_\mu^{\rm NME}$, $M_\mu^{\rm CME}$, and $M_{npγ,\mu}^{\rm PS}$. (iii) As defined in Eqs. (14), (16), (17), and (20), four additional amplitudes are introduced. Each of these amplitudes plus the TuTts amplitude $M_\mu^{\rm TuTts}$ are used to calculate $np\gamma$ cross sections at 225 MeV, for scattering angles lying between 12° and 43°. The results were used to systematically investigate the $np\gamma$ process. Our study focused on meson exchange current effects in $np\gamma$. The most important findings can be summarized as follows: (i) the two independent relativistic amplitudes, $M_{npγ,\mu}^{\rm PS}$ and $M_\mu^{\rm TuTts}$, predict quantitatively similar $np\gamma$ cross sections, which are generally consistent with the measured data in Ref. [1]. However, there remains a discrepancy between theory and experiment in some cases. The cause remains unclear, but it seems unlikely that the various theoretical models would have any common deficiencies. (ii) The anomalous magnetic moments, κ_p and κ_n, play an insignificant role in the $np\gamma$ process, because their contribution is negligibly small. (iii) The MEC effect is found to be significant when the two nucleon scattering angles are far from the elastic limit and insignificant when the nucleon scattering angles approach the elastic limit. (iv) The amplitude $M_\mu^{\rm CME}$ was identified as the origin of significant MEC effects, and the amplitude $B_\mu^{\rm CME}$ was identified as the leading MEC amplitude. We observed that $B_\mu^{\rm CME}$ also dominates the $np\gamma$ cross section for small angle scattering, primarily because of the fact that $g_{\rm A^+}^2 = 2g_{\rm A^0}^2$.

These findings have enhanced our understanding of the fundamental emission mechanism governing the $np\gamma$ process, especially the meson exchange current effect. Our approach to this investigation should prove useful in gaining further knowledge of the bremsstrahlung process.

ACKNOWLEDGMENTS

The work of M.K.L. and W.M.S. was supported in part by the CUNY Professional Staff Congress-Board of Higher Education Research Award Program. The work of B.F.G. was carried out under the auspices of the National Nuclear Security Administration of the US Department of Energy at Los Alamos National Laboratory under contract no. DE-AC52-06NA25396.

[1] Y. Safkan, T. Akdogan, W. A. Franklin, J. L. Matthews, W. M. Schmitt, V. V. Zelivinsky, P. A. M. Gram, T. N. Taddcucci, S. A. Wender, and A. F. Pate, Phys. Rev. C **75**, 031001(R) (2007).
[2] M. K. Liou and M. I. Sobel, Phys. Rev. C **4**, 1507 (1971).
[3] V. R. Brown and J. Franklin, Phys. Rev. C **8**, 1706 (1973).
[4] V. Herrmann, J. Speth, and K. Nakayama, Phys. Rev. C **43**, 394 (1991).
[5] K. Nakayama, Phys. Rev. C **39**, 1475 (1989).
[6] M. K. Liou, T. D. Penninga, R. G. E. Timmermans, and B. F. Gibson, Phys. Rev. C **69**, 011001(R) (2004).
[7] R. G. E. Timmermans, T. D. Penninga, B. F. Gibson, and M. K. Liou, Phys. Rev. C **73**, 034006 (2006).
[8] R. G. E. Timmermans, B. F. Gibson, Y. Li, and M. K. Liou, Phys. Rev. C **65**, 014001 (2001).
[9] Y. Li, M. K. Liou, R. G. E. Timmermans, and B. F. Gibson, Phys. Rev. C **58**, R1880 (1998).
[10] M. K. Liou, R. G. E. Timmermans, and B. F. Gibson, Phys. Rev. C **54**, 1574 (1996).
[11] M. K. Liou, Y. Li, W. M. Schreiber, and R. W. Brown, Phys. Rev. C **52**, R2346 (1995).
[12] Y. Li, M. K. Liou, and W. M. Schreiber, Phys. Rev. C **57**, 507 (1998).
[13] Y. Li, M. K. Liou, and W. M. Schreiber, Phys. Rev. C **72**, 024005 (2005).
[14] Y. Li, M. K. Liou, and W. M. Schreiber, Phys. Rev. C **64**, 064002 (2001).
[15] C. J. Horowitz, Phys. Rev. C **31**, 1340 (1985).